Geophysical Journal International

Geophys. J. Int. (2015) **202,** 901–913 doi: 10.1093/gji/ggv193
GJI Marine geosciences and applied geophysics

Finite element modelling of transient electromagnetic fields near steel-cased wells

Evan Schankee Um,[1] Michael Commer,[1] Gregory A. Newman[1] and G. Michael Hoversten[2]

[1] *Geophysics Department, Earth Sciences Division, Lawrence Berkeley National Laboratory, Berkeley, CA* 94720*, USA. E-mail: esum@lbl.gov*
[2] *Chevron Energy Technology Company, CoRE Leveraged Research, San Ramon, California, CA* 94583*, USA*

Accepted 2015 May 6. Received 2015 May 5; in original form 2015 January 14

SUMMARY

Wells and boreholes are routinely steel-cased in oil and gas fields and geological storage sites. There have been a number of studies on the effects of a steel-cased well on various electrical and electromagnetic (EM) geophysical methods. In this paper, we examine the use of a steel-cased well as a virtual vertical electric source for sensing deep localized resistive (e.g. CO_2, oil and gas) and conductive (e.g. conductive-proppant-filled fractures) targets when concentric electric sources are grounded around the collar of the well. To simulate the casing effects, we present a 3-D finite-element time-domain (FETD) algorithm with tetrahedral elements. The FETD algorithm is designed to reduce memory usage in adaptive time stepping by utilizing parallel direct and iterative solvers appropriately together. To avoid a larger number of tiny elements required for discretizing a thin wall of the casing, the hollow casing is approximated with a rectangular prism. By not discretizing the thin wall of and the curvature of the round casing, the approximation not only reduces the number of unknowns by an order of magnitude but also improves overall mesh qualities. We show that surface EM responses over the hollow casing and the prism are practically the same. Through FETD modelling of a rectangular prism as an approximation of a steel casing, we demonstrate that a steel casing can serve as a conduit through which a high concentration of electrical currents can flow downward from the surface, interact with deep localized reservoirs/fractures and produce a measurable perturbation in the surface EM fields. Concentric electric sources can further improve both the sensitivity to the deep targets and the overall magnitude of surface EM fields.

Key words: Numerical approximations and analysis; Downhole methods; Electromagnetic theory.

INTRODUCTION

3-D numerical modelling of a steel casing in electromagnetic (EM) geophysics has been studied in past decades. Early analyses on the effects of the steel casing on EM responses were mainly based on integral equation (IE) methods (Kaufman 1990; Schenkel & Morrison 1990; Wu & Habashy 1994). The IE methods utilize the symmetry of the casing and can efficiently model localized simple geometric structures. Finite difference (FD) methods are generally versatile and can simulate a casing-embedded complex earth model. However, FD modelling of the steel casing is still considered challenging due to several numerical difficulties. First, because of its high (e.g. 10^6–10^7 S m^{-1}) conductivity and thin (e.g. a few centimetres) wall, its FD modelling requires an extremely fine (millimetre scale) spatial discretization, resulting in a significant number (e.g. a few ten millions) of unknowns in a matrix system. The resulting computation cost is often intractable unless a scalable FD algorithm is used on a large-scale parallel computer (Commer & Newman 2004; Commer *et al.* 2015). Second, mixing high-conductivity cells of steel casings with low conductivity of the air can make a system matrix of FD equations ill-conditioned (Hördt & Müller 2000). When such fine cells are coupled with large cells used for modelling reservoir-scale and regional-scale geology, the resulting system matrix can be further ill-conditioned and pose a convergence issue with iterative solvers (Newman & Alumbaugh 1995).

Finite element (FE) modelling has also been used to simulate casing effects and has similar modelling challenges to those mentioned above. Due to prohibitive computational costs, 2-D and 2.5-D FE modelling has been common. For example, Lee *et al.* (2005) and Kim & Lee (2006) develop an FE method in the frequency-domain and analyse EM fields in a non-uniform steel-cased borehole. Pardo & Torres-Verdín (2013) use an adaptive *hp* FE method (Pardo *et al.* 2007), where *h* and *p* are an element size and the polynomial order of interpolation, respectively, and analyse the

Published by Oxford University Press on behalf of The Royal Astronomical Society 2015. This work is written by (a) US Government employee(s) and is in the public domain in the US.

Downloaded from https://academic.oup.com/gji/article/202/2/901/591436 by guest on 20 August 2022

sensitivity of a borehole EM system to hydraulic fractures in a steel-cased horizontal well. In these examples, they choose the cylindrical coordinate system and assume the cylindrical symmetry of conductivity distributions about the casing. Thus, an anomalous zone is modelled as a disk perpendicular to the casing. At the expense of the limited modelling complexity, the FE modelling approaches can be carried out without requiring significant computing resources.

In this paper, we present a full 3-D finite-element time-domain (FETD) algorithm for modelling casing effects. The FETD algorithm is designed to efficiently solve a large-scale FE problem in the time domain resulting from steel-casing-embedded earth models. The FETD algorithm utilizes unstructured tetrahedral meshes and can precisely discretize a round casing with small elements. Unlike FDTD algorithms with structured rectangular grids, the small elements do not extend to the computational boundaries, but their sizes can progressively increase outwards from the casing. Owing to the unstructured nature of tetrahedral meshes, the FETD algorithm is expected to be suited to simulating casing effects even when cased wells and anomalous structures do not confirm to the rectangular grids.

Major difficulties of 3-D FETD modelling for the casing effects include (1) a large number of unknowns resulting from a long (e.g. a few kilometres) and thin (e.g. a few centimetres) hollow casing, and (2) reliable and efficient mesh generation. Although tetrahedral meshes are expected to economically discretize a casing-embedded earth model, the discretization still requires a large number of elements (i.e. unknowns). The large number of unknowns is a particular concern because FETD algorithms require directly solving the system of FE equations at every time step regardless of implicit or explicit time discretization (Gockenbach 2002). In addition, as will be discussed later, an adaptive time-step control approach used in our FETD algorithm further increases the memory requirement by a factor of two (Um *et al.* 2010). It is also challenging to generate good-quality meshes when a kilometre-scale long and centimetre-scale thin casing structure needs to be discretized. In this case, a mesh generator needs to split a number of poor-quality tetrahedral elements inside and outside the casing into smaller good-quality ones. This splitting process requires long computation times and large storage. In certain circumstances, the splitting process fails to generate smaller and well-rounded elements, leaving the poor-quality elements in the final mesh. Such elements can be a source of numerical noises in FETD solutions.

In this paper, our FETD modelling algorithm and meshing strategy are designed to address the two major difficulties mentioned above. First, to manage a large problem size, the FETD algorithm utilizes both direct and iterative solver appropriately together, prevents the memory usage from being doubled during the adaptive time stepping. Thus, the memory usage is kept the same through the FETD computation. To further reduce a large number of elements (i.e. unknowns) required for representing a hollow steel casing, the casing is approximated with a simple prism. We demonstrate that surface EM responses over the casing and its corresponding prism agree well with each other. As will be shown later, the choice of the prism model over the hollow-casing model not only significantly reduces the number of unknowns but also improves mesh qualities and reduces mesh generation time.

Using the FETD algorithm with the prism representation of a hollow steel casing, we simulate and analyse surface transient EM (TEM) fields when both electric dipole sources and receivers are grounded in the vicinity of a steel-cased well. As mentioned in Hoversten *et al.* (2014) and Commer *et al.* (2015), a motivation beyond this numerical experiment is the possibility that the steel casing can serve as a direct conduit through which a high concentration of electrical currents can flow downward, directly interact with deep localized fractures and produce a measurable perturbation in the surface TEM fields. One can also consider crosswell EM systems to interrogate such fractures (Kim *et al.* 2014). However, new boreholes/wells would not be available because of prohibitive drilling costs in oil and gas fields and potential risks of leakages in hazardous waste monitoring sites. Therefore, it is worth to maximally utilize existing wells for better characterizing deep targets. Here, we further expand on the works of Hoversten *et al.* (2014) and Commer *et al.* (2015) by demonstrating that a multi-source configuration around a steel-cased well can significantly improve both the sensitivity to the deep targets and the signal-to-noise ratio of surface TEM fields.

The remainder of this paper is organized as follows. First, we present a 3-D FETD algorithm designed to efficiently handle a large number of unknowns resulting from the discretization of a long steel casing. Using the FETD algorithm, we demonstrate that a hollow steel casing can be approximated with a simple prism. The accuracy of the approximation and its computational benefits are discussed. Based on the approximation, we simulate surface TEM fields in the vicinity of a steel-cased well whose one end point is at the air-earth interface and the other end point is directly connected with either a resistive (e.g. oil, gas and CO_2) reservoir or a conductive (e.g. graphite-coated sand proppant filled) fractured zone. In order to boost the sensitivity and the signal strength, we simulate the simultaneous excitation of multiple dipole sources that are concentrically arrayed around the collar of a steel-cased well. The resultant sensitivity and detectability are compared with those of a single source configuration.

FETD SOLUTION STRATEGIES FOR LARGE-SCALE PROBLEMS

In this section, we briefly describe some key features of the FETD algorithm used for simulating the casing effects. To simulate TEM fields, we apply the standard Galerkin method to the electric field diffusion equation as described in details in Um *et al.* (2010, 2013) and get a system of FETD equations given as

$$\mathbf{C}^k \frac{\mathrm{d}\mathbf{u}^k(t)}{\mathrm{d}t} + \mathbf{P}^k \mathbf{e}^k(t) + \mathbf{s}^k = 0, \tag{1}$$

where

$$(i, j)\text{ element of conductivity matrix } \mathbf{C}^k = \iiint_{V^k} \sigma^k \mathbf{n}_i^k(\mathbf{r}) \cdot \mathbf{n}_j^k(\mathbf{r}) \mathrm{d}V, \tag{2}$$

$$(i, j)\text{ element of permeability matrix } \mathbf{P}^k = \iiint_{V^k} \frac{1}{\mu} \nabla \times \mathbf{n}_i^k(\mathbf{r}) \cdot \nabla \times \mathbf{n}_j^k(\mathbf{r}) \mathrm{d}\mathbf{V}, \tag{3}$$

$$i\text{ element of source vector } \mathbf{s}^k = \iiint_{V^k} \mathbf{n}_i^k(\mathbf{r}) \cdot \frac{\partial \mathbf{j}_s(\mathbf{r}, t)}{\partial t} \mathrm{d}V, \tag{4}$$

$$\text{unknown electric field vector } \mathbf{e}^k = \begin{bmatrix} e_1^k & e_2^k & \dots & e_6^k \end{bmatrix}, \tag{5}$$

μ is the magnetic permeability tensor, $\boldsymbol{\sigma}$ is the electric conductivity tensor and $\mathbf{j}_s$ is an impressed electric current source. $\mathbf{n}_i(\mathbf{r})$ is the first-order edge elements (Nédélec 1986). V is a volume of an

Downloaded from https://academic.oup.com/gji/article/202/2/901/591436 by guest on 20 August 2022

individual tetrahedral element. The superscript k and the subscript i denote the kth tetrahedral element and the ith edge of the element.

Eq. (5) is discretized using the second-order backward Euler method, resulting in the final FETD formulation:

$$\mathbf{A}^k(\Delta t)\mathbf{e}^k_{n+2} = \mathbf{C}^k\left(4\,\mathbf{e}^k_{n+1} - \mathbf{e}^k_n\right) - 2\Delta t\mathbf{s}^k_{n+2}$$
$$\text{where } \mathbf{A}^k(\Delta t) \equiv 3\mathbf{C}^k + 2\Delta t\mathbf{P}^k. \tag{6}$$

After systems of FETD equations from each element are assembled into a single large system of FETD equations (i.e. the global version of eq. 6), the superscript k is dropped. We apply the homogeneous Dirichlet boundary conditions to the boundaries of the computational domain, removing the external edges that consist of the surfaces of the computational domain from eq. (6). The final global system matrix is symmetric positive definite. Cholesky factorization (Saad 2003) can be effectively used to solve eq. (6).

An efficient solution strategy for eq. (6) is to utilize both the time invariance of matrix $\mathbf{A}$ with a constant Δt and the attenuation of TEM fields over time (Um *et al.* 2010). For example, the time-stepping procedure of eq. (6) starts with a small Δt. The initial matrix factorization is reused as long as Δt remains constant. The computational cost of each time step is simply that of backward and forward substitution. As high-frequency TEM fields are increasingly attenuated over time, a larger Δt can be used. To check if a new larger Δt can be used without affecting the accuracy of the solution, the solutions are computed at a given time twice: one with Δt and the other with $\alpha\Delta t$ where α is larger than 1 and typically set to 2. To do this, it is required to have the factors of both $\mathbf{A}(\Delta t)$ and $\mathbf{A}(\alpha\Delta t)$. If a norm of the difference of the two solution vectors is smaller than a tolerance that is empirically determined and is typically smaller than 10^{-4}, Δt is updated with $\alpha\Delta t$, and $\mathbf{A}(\Delta t)$ is discarded. Otherwise, the current Δt is kept. Thus, by successively introducing a larger Δt at particular intervals and re-factorizing $\mathbf{A}(\alpha\Delta t)$, one can speed up FETD solution processes. This approach is summarized in Fig. 1(a).

Using the adaptive time-stepping technique that leads to fast FETD computation, the FETD algorithm above has been successfully employed to analyse the effects of complex seafloor topography on TEM fields (Um *et al.* 2012) and to monitor water flooding in a reservoir (Colombo & McNeice 2013). Its parallel versions have been presented and proven scalable (Fu *et al.* 2015). However, its major drawback is the fact that the approach doubles peak memory usage. The increased memory usage may not be a serious issue for small-to-medium-scale modelling problem with a number of unknowns smaller than a few millions. However, the increased memory usage is a particular concern in this study because the fine discretization of a thin (e.g. a few ten centimetres) and long (e.g. a few kilometres) casing can result in a large number of unknowns (e.g. about 10 million unknowns even with a 200 m long casing) as will be shown later. Along with the fine discretization, Cholesky factorization requires a very large amount of memory. Thus, it is important not to double peak memory usage in adaptive time stepping.

To mitigate the memory overhead for the adaptive time-stepping technique, we adopt a hybrid use of direct and iterative solvers as shown in Fig. 1(b). As done in Fig. 1(a), we first complete the Cholesky factorization for a given Δt and start the time-stepping process. Later, in order to check if $\alpha\Delta t$ is acceptable, we do not factorize $\mathbf{A}(\alpha\Delta t)$. Instead, we employ the conjugate gradient (CG) method for solving eq. (6) with $\alpha\Delta t$. The current Cholesky factor of $\mathbf{A}(\Delta t)$ is used as a pre-conditioner for the CG method. We have found that if α is not too large (e.g. $\alpha \gg 2$), the Cholesky factor of $\mathbf{A}(\Delta t)$ can serve as an effective CG pre-conditioner for eq. (6) with $\alpha\Delta t$. This is analogous to an observation in the frequency (f) domain that the factor of $\mathbf{A}(f)$ can be effectively used to pre-condition $\mathbf{A}(\alpha f)$ as shown in Um *et al.* (2013). If solutions of eq. (6) corresponding to Δt and $\alpha\Delta t$ agree with each other within a tolerance bound, $\alpha\Delta t$ is accepted as a new Δt. Then, we discard the factor of $\mathbf{A}(\Delta t)$ and compute a new factor of $\mathbf{A}(\alpha\Delta t)$ without doubling the peak memory usage. Alternatively, we can completely switch from the Cholesky direct solver to the CG solver and continue to use the factor of $\mathbf{A}(\Delta t)$ as the pre-conditioner for eq. (6) with $\alpha\Delta t$ as long as FETD solutions converge within a reasonable number of iterations. In this way, we use 50 per cent amount of memory required for Fig. 1(a).

Until now, we have described the adaptive time-stepping FETD algorithm that is suited to a problem with a large number of unknowns. In our implementation of the FETD algorithm, we utilize a parallel factorization and triangular solver, MUMPS (Amestoy *et al.* 2001, 2006). The MUMPS solver is used together with a parallel pre-conditioned CG solver found in PETSC library (Balay *et al.* 2014). Earth models with steel casings are discretized with tetrahedral elements using TetGen mesh generator (Si 2013). In the next sections, we analyse the TEM responses to deep 3-D targets in the vicinity of a long steel casing. Along with the modelling analysis, we summarize the overall computational cost associated with the

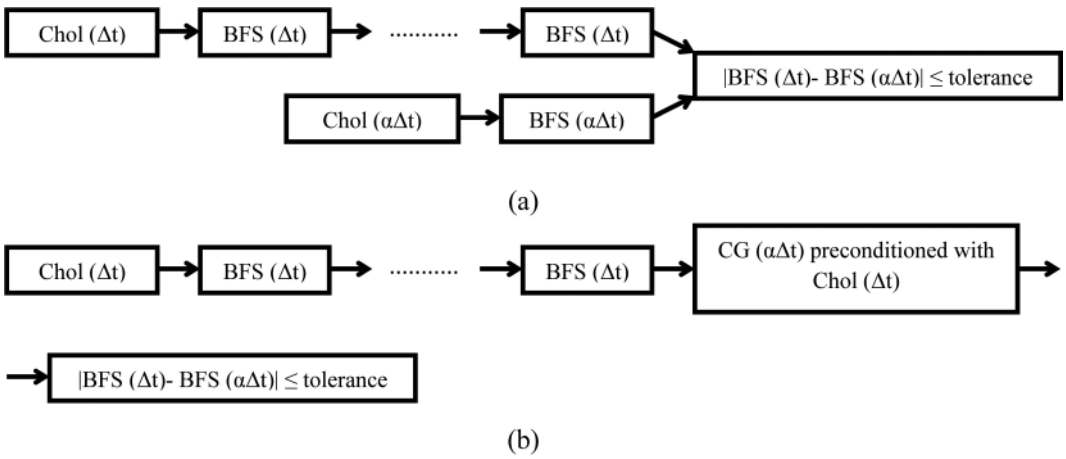

Figure 1. (a) The adaptive time-stepping technique shown in Um *et al.* (2010). (b) The new adaptive time-stepping technique with the hybrid use of direct and iterative solvers. Chol, BFS and CG represent Cholesky factor, backward/forward substitution and conjugate gradient solver, respectively.

Downloaded from https://academic.oup.com/gji/article/202/2/901/591436 by guest on 20 August 2022

modelling, demonstrating that it is practically feasible to directly discretize a long steel-cased well and simulate its TEM responses in a reasonable time frame.

APPROXIMATION OF HOLLOW STEEL CASING WITH PRISM

Before we study the role of a steel casing as a virtual vertical source for sensing reservoirs and fractures, we examine the discretization rules of the steel casing and verify the accuracy of the FETD solutions through their comparisons with reference solutions. As a general rule, tetrahedral elements are smallest near a source and gradually grow away from the source. The growth rate is empirically determined but is usually less than or equal to a factor of two from one edge to the next. In addition, the element size should be fine around the casing due to its thin wall and the high-conductivity contrast between the casing and its surround media. Furthermore, because the FETD algorithm uses the homogeneous Dirichlet boundary condition, the boundaries of the computational domain should be sufficiently distant away from sources and receivers. For more details and examples, a reader is referred to Um *et al.* (2010, 2012).

We first consider a hollow steel casing embedded into a uniform lower half-space (0.033 S m^{-1}). The round casing features a wall thickness of 12.223 mm, a diameter of 135 mm (to the outer wall) and a conductivity of 10^6 S m^{-1}. Its relative permeability is set to 1. The circumference of the casing is approximated using 36 edges of the same length. The vertical casing starts from $z = 0$ m (i.e. the air–earth interface) and extends down to 200 m in depth. The FETD discretization of the hollow-casing model is shown in Fig. 2(a). To ensure overall good mesh qualities for this particular discretization, we utilize two quality measures for tetrahedral elements (Si 2013).

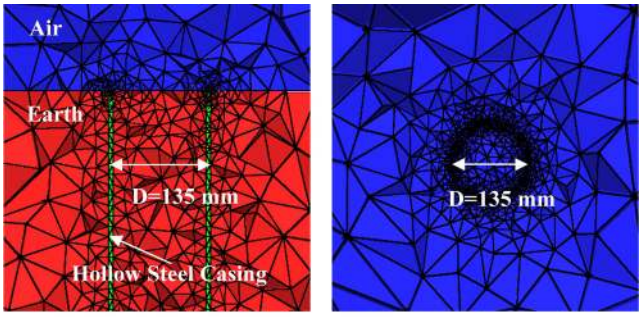

(a) The *xz* view (left) and the *xy* view (right).

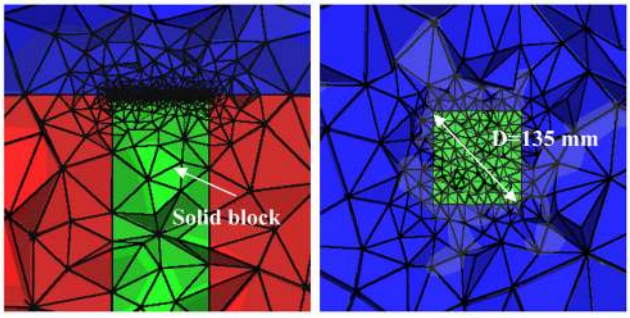

(b) The *xz* view (left) and the *xy* view (right).

Figure 2. Cross-sectional views of a central portion of (a) the hollow steel-casing FETD model and (b) the rectangular prism FETD model.

First, we enforce the maximum radius–edge ratio of a tetrahedron (i.e. the ratio of the radius of its circumscribed ball to the length d of its shortest edge) to be equal to or smaller than 1.5. Second, the minimum allowable dihedral angle (i.e. an angle between two facets of a tetrahedron) is set to 10°. The quality of the resulting meshes is examined by a mesh quality factor (COMSOL 2008) defined as

$$q = \frac{72\sqrt{3}V}{\left(h_1^2 + h_2^2 + h_3^2 + h_4^2 + h_5^2 + h_6^2\right)^{3/2}}, \tag{7}$$

where V is the volume of a tetrahedral element, h_i is the length of the ith edge of the element.

The mesh quality factor has been successfully used to evaluate meshes for marine controlled-source EM modelling (Um *et al.* 2012) and proven as an effective measure for diffusive EM modelling. For a regular tetrahedral element (i.e. an equilateral tetrahedral element), q is equal to 1. It is known that when q is equal to or greater than 0.1, shapes of the elements do not affect solution accuracy.

It took about 20 min to generate the meshes on a 1.4 GHz single core AMD Opteron processor. The resulting meshes consist of 8 421 559 tetrahedral elements. It turns out that 44 of 8 421 559 elements have quality factors smaller than 0.1. However, the elements are distant from a central portion of the computational domain where sources, receivers and the casing are placed. The average quality factor of the 44 elements is not too low but is about 0.077. Although it is not ideal to have the low-quality elements in the computational domain, it is our experience that such elements do not propagate serious numerical noises to FETD solutions. The model has 9 778 426 unknowns.

To simulate the effects of the steel casing on surface TEM responses, a 10-m long x-oriented electric dipole source is excited 50 m distant from the casing. Receivers are placed along the x-axis. The FETD solution processes consist of 9 Cholesky factorizations and 893 time steps. In the adaptive time stepping, the pre-conditioned CG solver typically converges within 10 iterations. Run time for the FETD solution is 347 min using 120 cores of Intel Xeon® processors with 480 GB memory. As a side note, the run time for the FETD solution to the uniform half-space without the casing is trivial. We were able to simulate the electric field responses over the same range of time in 20 min with a single core of Intel i7 processor and 16 GB memory. The comparison highlights the direct modelling cost of the hollow steel casing.

The electric field responses at selected receiver positions are plotted in Fig. 3(a) and are compared with reference FDTD solutions for verification. In the reference FDTD model, the curvature of the steel casing is discretized with 12.223 mm cells. The validity of the FDTD solutions to the steel casing model has been examined in details in Commer *et al.* (2015). As shown in Fig. 3(a), both FETD and FDTD solutions show good agreements. The FETD algorithm and the FDTD algorithm have their own adaptive time-stepping methods and produce the solutions at different time axes. Thus, the two solutions are interpolated on the same time axis to plot the relative differences of the two solutions as shown in Fig. 3(b). Except the large relative difference at $x = 11$ m due to a sign reversal, the relative errors in late times are bounded within about 5 per cent. Note that neither the FDTD solutions nor the FETD solutions are absolute reference solutions. Based on different spatial and temporal discretization approaches and solution processes, each solution has its own errors. In this study, we do not attempt to examine the individual error sources of each solution for further reducing the differences. Instead, we simply conclude that the two solutions show

Downloaded from https://academic.oup.com/gji/article/202/2/901/591436 by guest on 20 August 2022

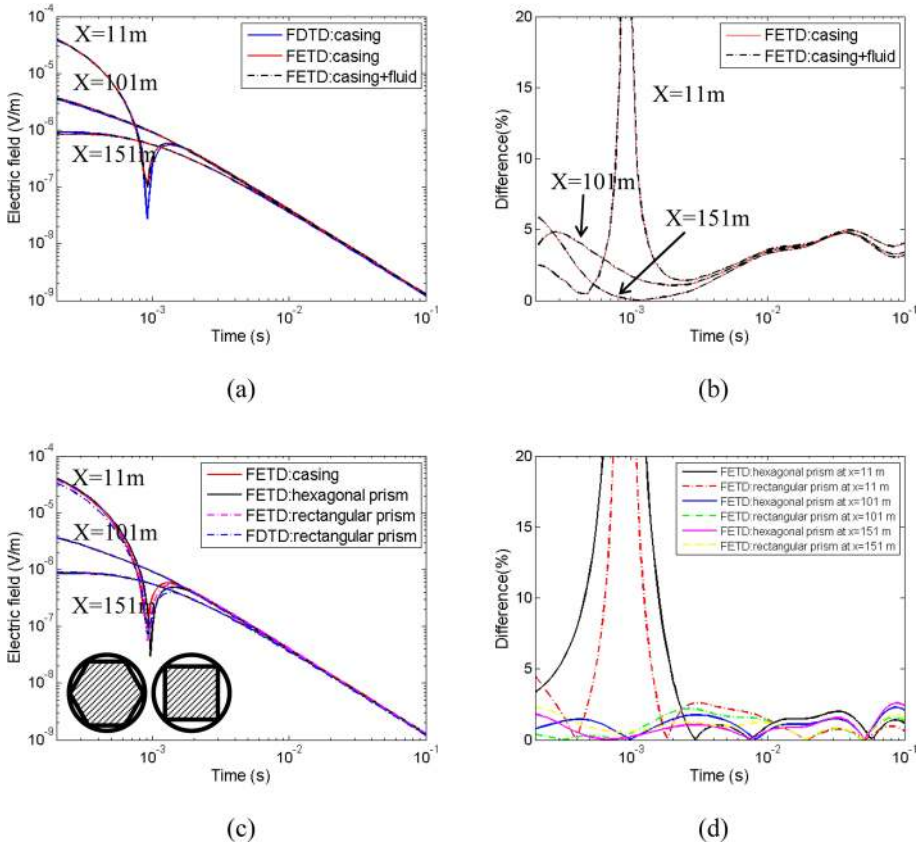

Figure 3. (a) The surface electric field responses over the 200 m vertical casing that is embedded into the uniform half-earth model. (b) The relative differences of the FETD solutions with respect to the FDTD solutions. (c) The comparison of the hollow-casing model and its corresponding prism models. The cross-sectional views of the solid hexagonal prism model and the rectangular prism model are shown at the lower left corner of (c). (d) The relative differences of the FETD prism models with respect to the FETD casing model.

good enough agreements for numerical modelling studies because, as will be shown in the next two sections, a localized deep (e.g. 2 km) resistive/conductive target can produce anomalous responses a few hundred per cent larger than the difference of FDTD and FETD solutions.

As the steel-cased well is typically filled with drilling fluid, we also simulate TEM responses to the fluid-filled casing. The conductivity of the fluid is set to 0.33 S m^{-1}, which is an order of magnitude larger than that of the background medium. Figs 3(a) and (b) show that the fluid-filled casing model and the hollow-casing model produce the same surface responses. In other words, the conductivity inside the steel casing has little effects on the surface TEM responses. This observation can be explained with the fact that most transient electric currents would flow through the casing surfaces due to the large contrast of electrical conductivity between the casing and its surrounding medium. This observation implies that it is possible to approximate the hollow steel casing with a solid cylinder by removing the inner wall of the hollow steel casing. By avoiding discretizing the thin circular wall of the casing with tiny elements, we would significantly reduce the total number of elements required to represent the casing. The good agreements of the FETD and FDTD solutions also imply that it is not critically important to accurately represent the curvature of the steel casing when surface TEM fields are simulated. A key benefit of a coarse representation of the round casing is that it greatly reduces the total number of elements.

In order to check if the hollow casing can be replaced with a simple and easily discretizable object, we compare the hollow-casing responses with those from models with a solid rectangular prism and a hexagonal prism as shown in Fig. 3(c). The size of the prisms is equal to the outer diameter of the casing. Their conductivity is set to that of the casing. For verification, the surface TEM responses over the rectangular prism are computed using both the FETD algorithm and the FDTD algorithm. The FDTD algorithm divides (i.e. discretizes) the rectangular prism into four FD cells on the *xy* plane. Their size is set to 67.5 mm (half the diameter). As shown in Fig. 3(c), when a receiver is just 11 m distant from the prisms, the surface responses over the prism models do not agree well with those over the hollow-casing model. However, when a receiver is distant more than 100 m from the prisms, we see overall excellent agreements between the hollow-casing model and the prism models. The relative differences of the two prism model solutions with respect to the casing model solution are also plotted in Fig. 3(d). The relative differences are bounded within about 2 per cent in intermediate-late times (3×10^{-3} to 10^{-1} s), confirming that the prisms can be an alternative to the hollow casing.

The use of the prisms significantly reduces the computational burdens of casing modelling. For example, the number of elements and the number of unknowns for the rectangular prism model are 1 132 050 and 1 304 678, respectively. These numbers are about 13 per cent of those of the hollow-casing model. Owing to such reductions, we were able to simulate the prism model in 39 min with 30 cores of Intel Xeon® processors with 120 GB memory. The run time for generating tetrahedral meshes also reduces from about 20 min to 36 s. The short run time would make it practically possible to generate/update tetrahedral meshes in inverse modelling

Downloaded from https://academic.oup.com/gji/article/202/2/901/591436 by guest on 20 August 2022

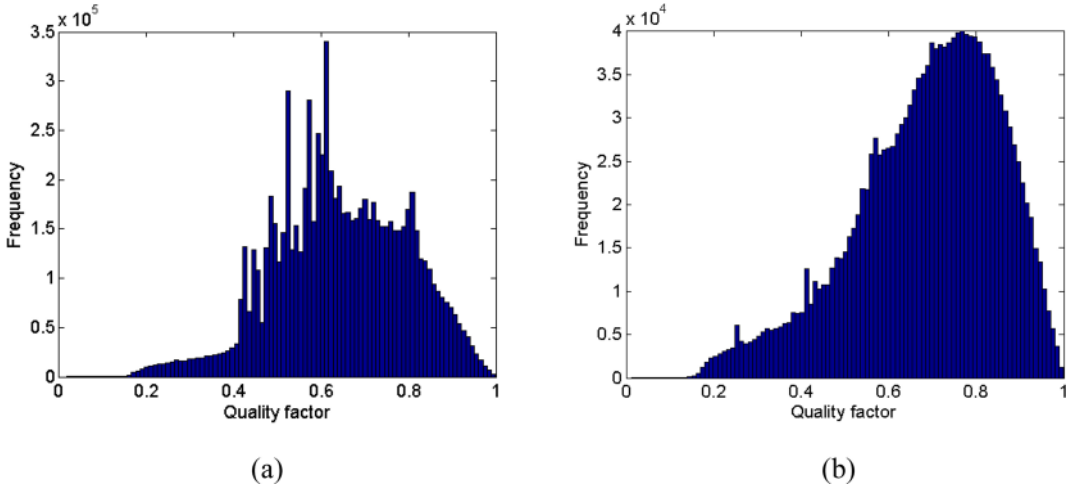

(a) (b)

Figure 4. The histogram of quality factors for the final tetrahedral meshes. (a) The hollow steel-casing FETD model. (b) The rectangular prism FETD model.

applications. The choice of the rectangular prism over the hollow casing also improved overall mesh qualities. For the prism model, all elements have quality factors larger than 0.1. Fig. 4 compares the histogram of the quality factor of eq. (7) between the hollow-casing model and the rectangular prism model. By avoiding tiny elements required for the thin hollow casing, more tetrahedral elements become close to the equilateral elements (quality factor = 1.0), improving the overall mesh quality.

As a final note, one might consider not only simplifying the geometry of a casing but also changing its properties. For example, one can attempt to increase the size of a prism and accordingly decrease its conductivity. The increased minimum size of elements and the decreased maximum conductivity would improve the condition number of an FETD system matrix. The attempt is similar to developing an effective medium theory for upscaling EM properties of a steel casing. We see some success in such efforts, but it has been our experience that it is difficult to maintain good agreements of true and approximate casing solutions at a wide range of casing-receiver offsets if multiple casing parameters simultaneously change. Thus, in this study, we approximate a hollow casing with a corresponding rectangular prism and fix its conductivity to that of the casing. Its role as a virtual vertical source will be examined in reservoir-scale models in the next two sections.

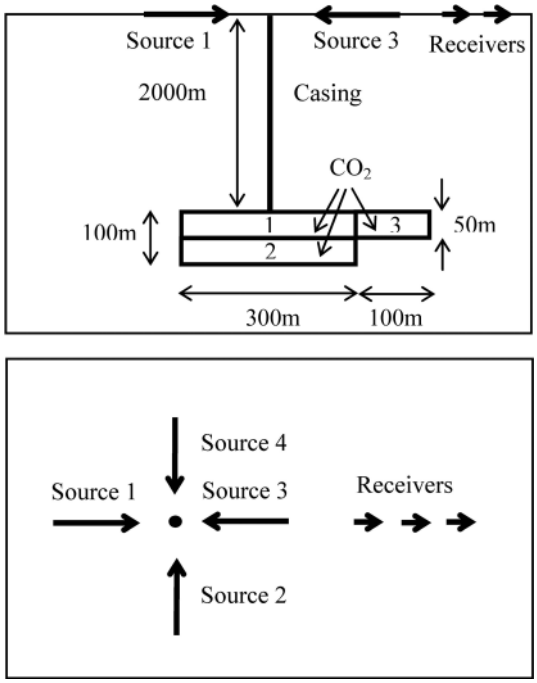

Figure 5. The cross-sectional (top) and plan (bottom) views of the wire-frame of the CO_2 reservoir models.

SENSITIVITY TO DEEP RESISTIVE CO_2 RESERVOIR

The first group of FETD simulations is performed for verifying the sensitivity of a surface TEM configuration to deep localized resistive CO_2 targets (Fig. 5 and Table 1). A 2-km long round steel casing features a wall thickness of 12.223 mm and an outer diameter of 135 mm. The casing is approximated by a rectangular prism with the side length equal to the outer diameter of the casing. The casing is vertically embedded into a uniform half-space (10^{-1} S m^{-1}). Note that it is not difficult for FETD modelling to accommodate complex background media. However, in these examples, we assume the uniform background medium to clearly highlight the effect of the steel casing on the targets. The conductivity of the air is set to 5×10^{-4} S m^{-1}.

The time-lapse changes of the CO_2 reservoir are shown in Fig. 5 and Table 1. The time-lapse models are designed to show vertical and horizontal changes of the reservoir. Before the injection, we assume the casing-embedded uniform half-space earth. As the CO_2 injection starts, a 50-m thick resistive (10^{-2} S m^{-1}) CO_2 block (block 1) is created. Later, the thickness of the reservoir increases from 50 to 100 m by combining blocks 1 and 2 into one. Finally, block 3 is added to the right side of block 1. The reverse time-lapse changes of the reservoir would be similar to a recovery scenario of hydrocarbon and gas. To highlight the role of the steel casing, we simulate the four stages of the CO_2 injection without (Models 1–4) and with (Models 5–8) the steel casing (Table 1). At each stage, we assume that the concentration of CO_2 is spatially uniform inside the blocks. Their conductivity values are uniformly set to 10^{-2} S m^{-1}. The conductivity value is slightly out of a typical range (3×10^{-2} to 3×10^{-1} S m^{-1}, a personal communication with Dr. Michael Wilt). Thus, one can consider the given modelling examples as a high contrast case.

Downloaded from https://academic.oup.com/gji/article/202/2/901/591436 by guest on 20 August 2022

Table 1. Eight earth models with and without the steel casing and CO_2 blocks.

Model	Description
Model 1	Uniform half-space
Model 2	Uniform half-space + CO_2 block 1
Model 3	Uniform half-space + CO_2 blocks 1 and 2
Model 4	Uniform half-space + CO_2 blocks 1, 2 and 3
Model 5	Uniform half-space + casing
Model 6	Uniform half-space + casing + CO_2 block 1
Model 7	Uniform half-space + casing + CO_2 blocks 1 and 2
Model 8	Uniform half-space + casing + CO_2 blocks 1, 2 and 3

Four independent or simultaneous dipole sources are considered as shown in Fig. 5. Each source is 50-m long and its polarization direction is towards the casing. The inner end point of the dipole source is 20 m distant from the casing. The ramp-off time of the dipole source is set to 10^{-4} s. The source current is set to 1 A. The array of x-oriented electric dipole receivers are placed along the positive x-axis. On average, the models consist of 5 962 179 tetrahedral elements and 6 891 427 unknowns. The FETD solution processes consist of 9 Cholesky factorizations and 893 time steps. The time-step size is successively doubled from 2×10^{-5} to 5.12×10^{-3} s. The average FETD run time is about 174 min using 120 cores of Intel Xeon® processors with 240 GB memory. On average, it takes about 87 s for TetGen to generate FETD meshes on a single core AMD Opteron processor 1.4 GHz. As a side note, it takes about 145 min to discretize the hollow steel casing. The resulting model consists of 59 199 999 elements. Thus, the use of the rectangular prism reduces the problem size by an order of magnitude.

Fig. 6 shows the inline electric field measurements with and without the steel casing when a single source (source 1) is turned off. Without the steel casing, the inline measurements fail to distinguish the four models (Models 1–4) each other. Relative differences of Model 1 and Models 2–4 are smaller than 0.2 per cent (not plotted in this paper). In contrast, when the steel casing is embedded into the earth model, it significantly changes overall shapes of sounding curves (the middle column in Fig. 6). The first sign reversals due to the near-surface steel casing (Commer *et al.* 2015) are observed in early times. The presence of the resistive CO_2 reservoirs makes the second reversals appear slightly early in intermediate times.

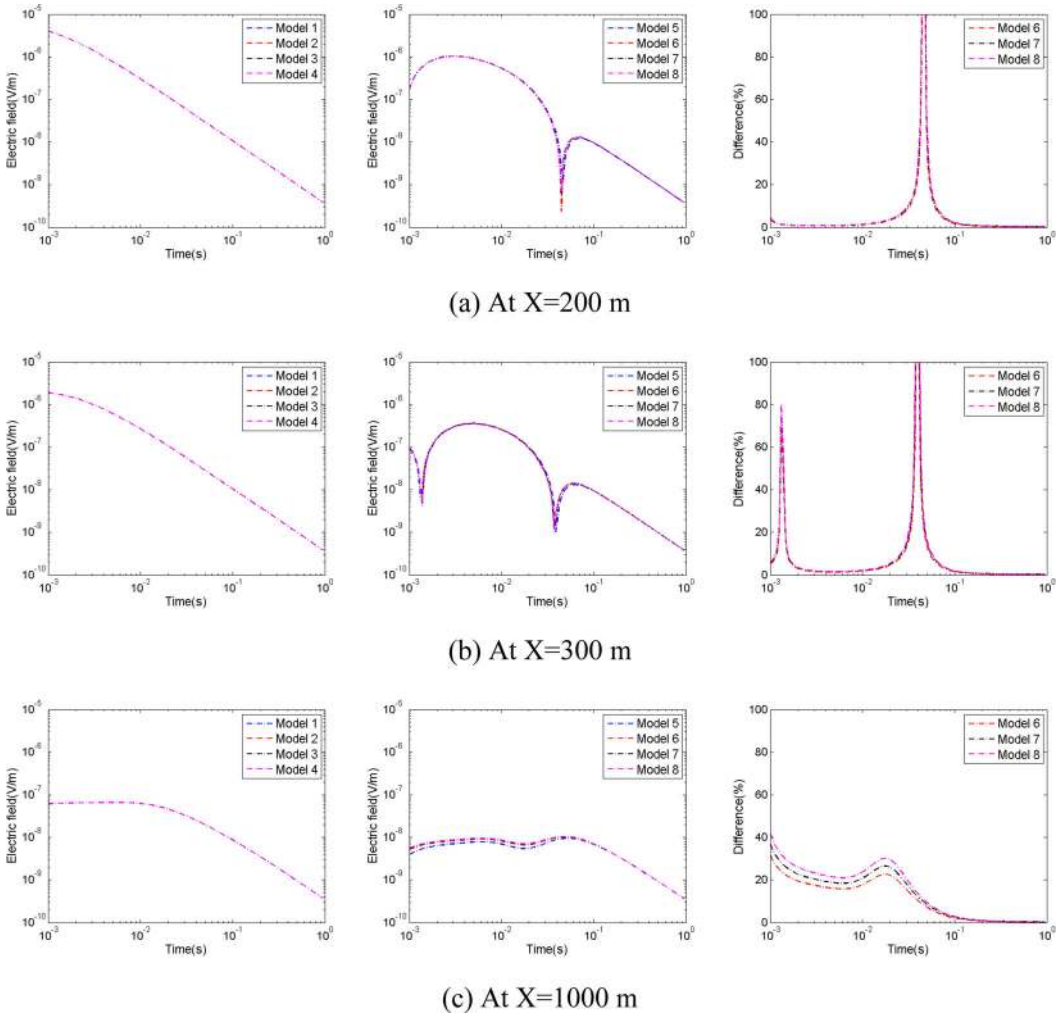

Figure 6. Responses to the CO_2 models with and without the casing (Fig. 5 and Table 1) at (a) 200 m offset, (b) 300 m offset and (c) 1000 m offset. A single source (source 1) is used. Model 1 is a background half-space model. Model 2 has a 50 m thick CO_2 reservoir block. In Model 3, the thickness of the block is doubled. In Model 4, the block extends in the x-direction by 100 m. Models 5–8 correspond to Models 1–4, respectively, except that Models 5–8 have the vertical casing at their centre. The left column shows horizontal electric field (E_x) responses when the steel casing is not embedded into the earth model (Models 1–4). The middle column shows E_x responses when the casing is embedded into the earth model (Models 5–8). The right column shows the relative E_x difference (%) of Model 5 and Models 6–8.

Downloaded from https://academic.oup.com/gji/article/202/2/901/591436 by guest on 20 August 2022

This temporal shift of the second reversals result in large relative differences between the reference model (Model 5) and the reservoir models (Models 6–8), demonstrating the increased sensitivity of the surface electric field measurements to the reservoirs.

Next, we examine the sensitivity of a multisource configuration to the CO_2 reservoirs when the configuration is deployed around the vertical steel casing. Four horizontal electric sources (Sources 1–4) are located concentrically around the steel casing as shown in Fig. 5. The sources are synchronized and are turned off simultaneously. The technical feasibility of this source layout has been demonstrated by Mogilatov & Balashov (1996) and Helwig *et al.* (2010). Before the four sources are turned off, the geometry of the initial direct current flow is similar to that of a vertical electric source embedded into the earth. After the turn-off, the high concentration of vertical currents at the centre diffuses directly downwards and interacts with the reservoirs. If the earth model has a vertical steel casing at the centre of the sources, the transient vertical currents will tend to reside in the steel casing and diffuse downwards very slowly due to the high electrical conductivity of the casing. The effect of this long-lasting vertical current can boost a virtual electric source created by the concentric dipole configuration, leading to the enhanced sensitivity to the reservoirs.

The resulting electric field measurements over the CO_2 models without the casing are compared in Fig. 7. Note that the measurements do not have the sign reversals in early times. Without the steel casing, the measurements show clear sensitivity to the three CO_2

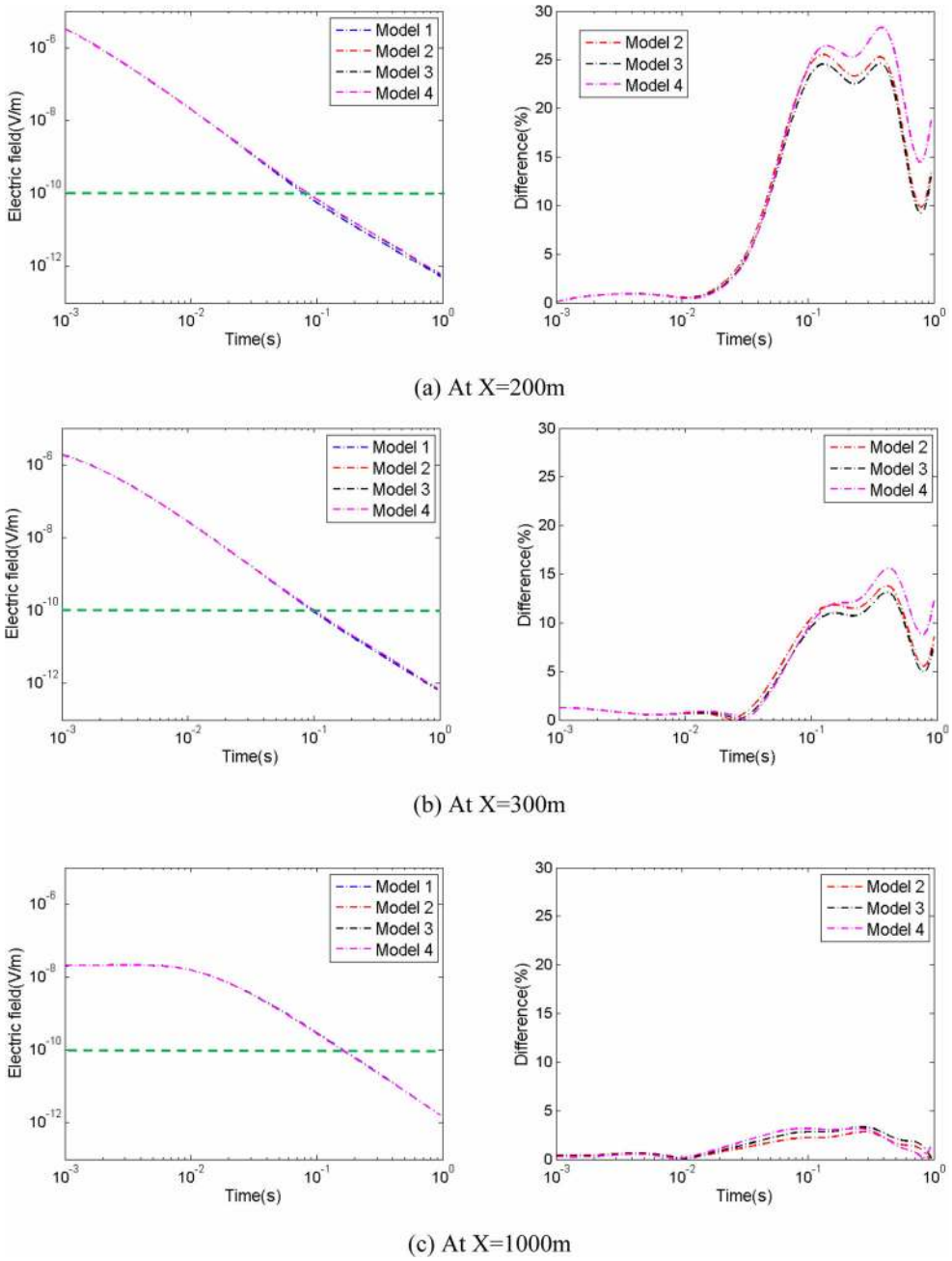

Figure 7. Responses to the CO_2 models without the steel casing (Fig. 5 and Table 1). Sources 1, 2, 3 and 4 are used simultaneously. The left column shows E_x responses over Model 1 (the uniform half-space model) and Models 2–4 (the CO_2 models) at (a) 200 m offset, (b) 300 m offset and (c) 1000 m offset. The right column shows the relative difference (%) of Model 1 and Models 2–4. The broken green lines indicate an assumed noise level.

Downloaded from https://academic.oup.com/gji/article/202/2/901/591436 by guest on 20 August 2022

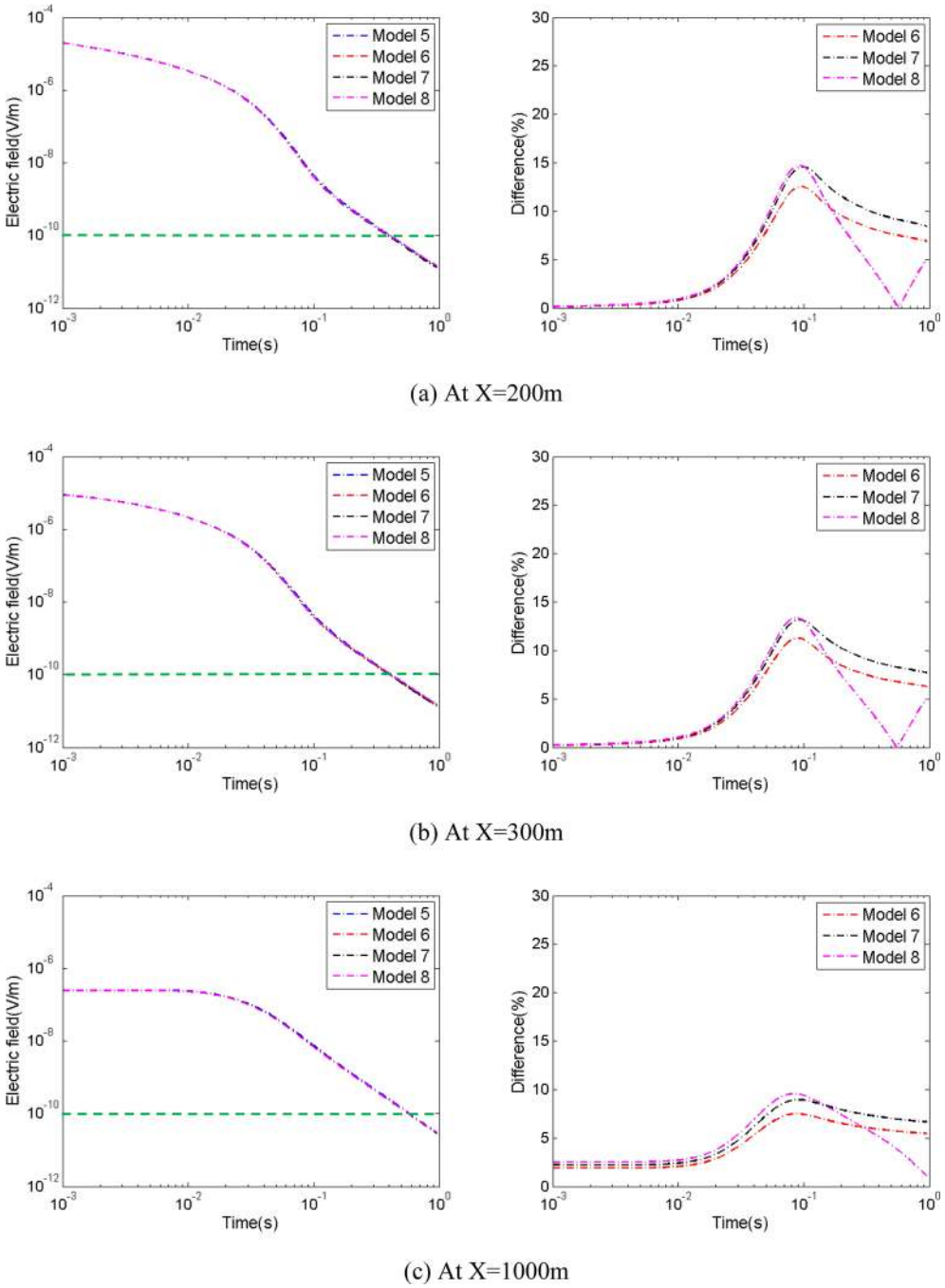

Figure 8. Responses to the CO_2 models with the steel casing (Fig. 5 and Table 1). Sources 1, 2, 3 and 4 are used simultaneously. The left column shows E_x responses over Model 5 (the casing-only model) and Models 6–8 (the casing and CO_2 models) at (a) 200 m offset, (b) 300 m offset and (c) 1000 m offset. The right column shows the relative difference (%) of Model 5 and Models 6–8. The broken green lines indicate an assumed noise level.

models. The steel casing further boosts the sensitivity to vertical and horizontal changes of the CO_2 reservoirs (Fig. 8). The casing also enhances the signal-to-noise ratio. For example, the presence of the steel casing makes the electric fields measurable until about 0.4 s (see the crossing of the sounding curves and the assumed noise level in Fig. 8). Without the steel casing, the electric fields are measurable only until about 0.1 s. Note that the discussion above about the signal-to-noise ratio is based on 1-A source. In practice, depending on ground conditions, one can inject a larger amount of source current (e.g. 10–100 A) and boost the measurements by a few orders of magnitude, making it possible to measure later-time responses from a deeper target. In short, the modelling examples clearly demonstrate the benefits of the casing-aided multisource configuration: the enhanced sensitivity and the improved signal-to-noise ratio.

SENSITIVITY TO DEEP CONDUCTIVE FRACTURED ZONE

The second group of FETD simulations demonstrates the sensitivity of the casing-aided surface source(s) to a deep conductive fractured zone as shown in Fig. 9. Sources and receivers are kept the same

Downloaded from https://academic.oup.com/gji/article/202/2/901/591436 by guest on 20 August 2022

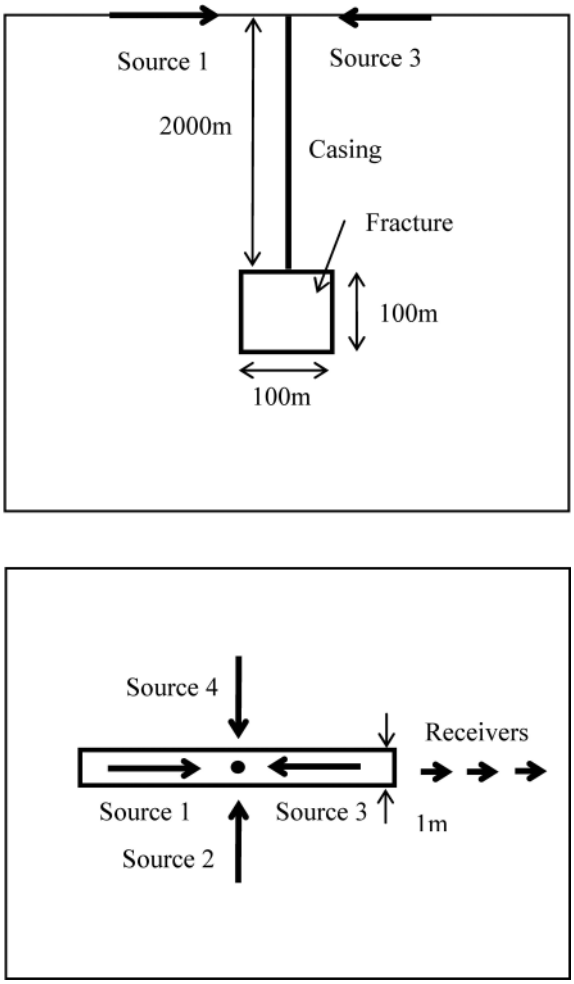

Figure 9. The cross-sectional (top) and plan (bottom) views of the wire-frame of the fracture model.

as in the previous example. The 2-km long steel casing features a wall thickness of 20 mm and an outer diameter of 257 mm. Again, the casing is approximated by a rectangular prism with the side length equal to the outer diameter of the casing. The conductivity of the casing is set to 5×10^6 S m^{-1}. The conductivity of the air and the background earth is set to 5×10^{-4} and 10^{-1} S m^{-1}, respectively. We consider a vertical fractured zone that is oriented in the *x*-direction and is placed directly below the lower end point of the casing without a gap. Its dimension is 100, 1 and 100 m in the *x*-, *y*- and *z*-directions, respectively. It is assumed that the fluids in the fractured zone contain a portion of highly conductive proppants such as graphite-coated sands (Hoversten *et al.* 2014). Thus, the conductivity of the fractured zone can also be highly conductive and is set to 125 S m^{-1}. The fractured zone is the realization of a thin conductive vertical fracture sheet whose dimension and conductivity are 100–0.05–100 m and 2500 S m^{-1}, respectively.

As a side note, the thin fracture sheet would be ideally modelled as a large (metre scale) anisotropic structure using an effective medium theory. Berryman & Hoversten (2013) present an effective medium theory for approximating the fracture as a set of ellipsoids saturated with fluids. Caudillo-Mata *et al.* (2014) propose an inversion-based effective medium theory. Heagy *et al.* (2014) assign physical properties to a set of fractures using an analytic approach with a few

Table 2. Four earth models with and without the steel casing and the fracture.

Model	Description
Model 9	Uniform half-space
Model 10	Uniform half-space + fracture
Model 11	Uniform half-space + casing
Model 12	Uniform half-space + casing + fracture

assumptions. We also attempted to apply to the casing-and-fracture model an effective medium theory (Commer & Newman 2008) that is based on parallel circuits. The effective medium theory has been proven robust to map geophysical properties from inverse modelling meshes (i.e. coarse imaging meshes) to forward modelling meshes (i.e. fine computational meshes) and vice versa. However, it is our overall experience that an effective medium theory should be applied carefully to a model that has an unusual large contrast (≥4∼5 orders of magnitude) of electrical properties due to casings and electromagnetically engineered fluids/proppants because their presence can make the validity of an effective medium theory vary from model to model. Although the anisotropic effective medium approach has potential to significantly improve a way for us to model fractures and steel casings, the evaluation of various effective medium theories for our casing-and-fracture model would go beyond the scope of this work. Rather, in this modelling example, our aim is very modest: to present the sensitivity analysis when the fracture sheet is modelled as a conductive isotropic structure in a volume-averaged sense.

To highlight the effects of the steel casing and the different source configurations on the sensitivity to the fractured zone, we consider four subsurface scenarios as described in Fig. 9 and Table 2. We simulate TEM responses over the four models with the inline configuration (i.e. Source 1) and with the concentric source array (Sources 1, 2, 3 and 4). On average, the models consist of 4 582 421 tetrahedral elements and 5 310 988 unknowns. The mesh generation is completed in about 157 s. The FETD solution processes consist of 9 Cholesky factorizations and 893 time steps. The time-step size is successively doubled from 2×10^{-5} to 5.12×10^{-3} s. The average FETD run time is about 125 min using 120 cores of Intel Xeon® processors with 240 GB memory.

Fig. 10 shows the electric field measurements with and without the casing when Source 1 is turned off. In contrast to the resistive reservoir in the previous example, the conductive fractured zone makes the sign reversal appear slightly late. This observation is consistent with the modelling result of Commer *et al.* (2015) where a horizontal conductive fracture also results in a delayed sign reversal in time. This temporal shift of the reversal is responsible for large relative differences of Models 11 and 12 as shown in Fig. 10. The signal strength is above the prescribed field noise level and is assumed measureable in practice.

Fig. 11 shows the electric field measurements resulting from the multisource configuration. When the multisource configuration involves the steel casing, both the signal strength and the sensitivity to the vertical fractured zone are boosted, resulting in 10–30 per cent perturbation in the surface electric field that would not be measured without the casing. In summary, although the multisource configuration is logistically challenging in practice (Mogilatov & Balashov 1996; Goldman *et al.* 2015), our examples clearly demonstrate potential benefits of the multisource configuration for sensing deep localized targets around the cased well.

Downloaded from https://academic.oup.com/gji/article/202/2/901/591436 by guest on 20 August 2022

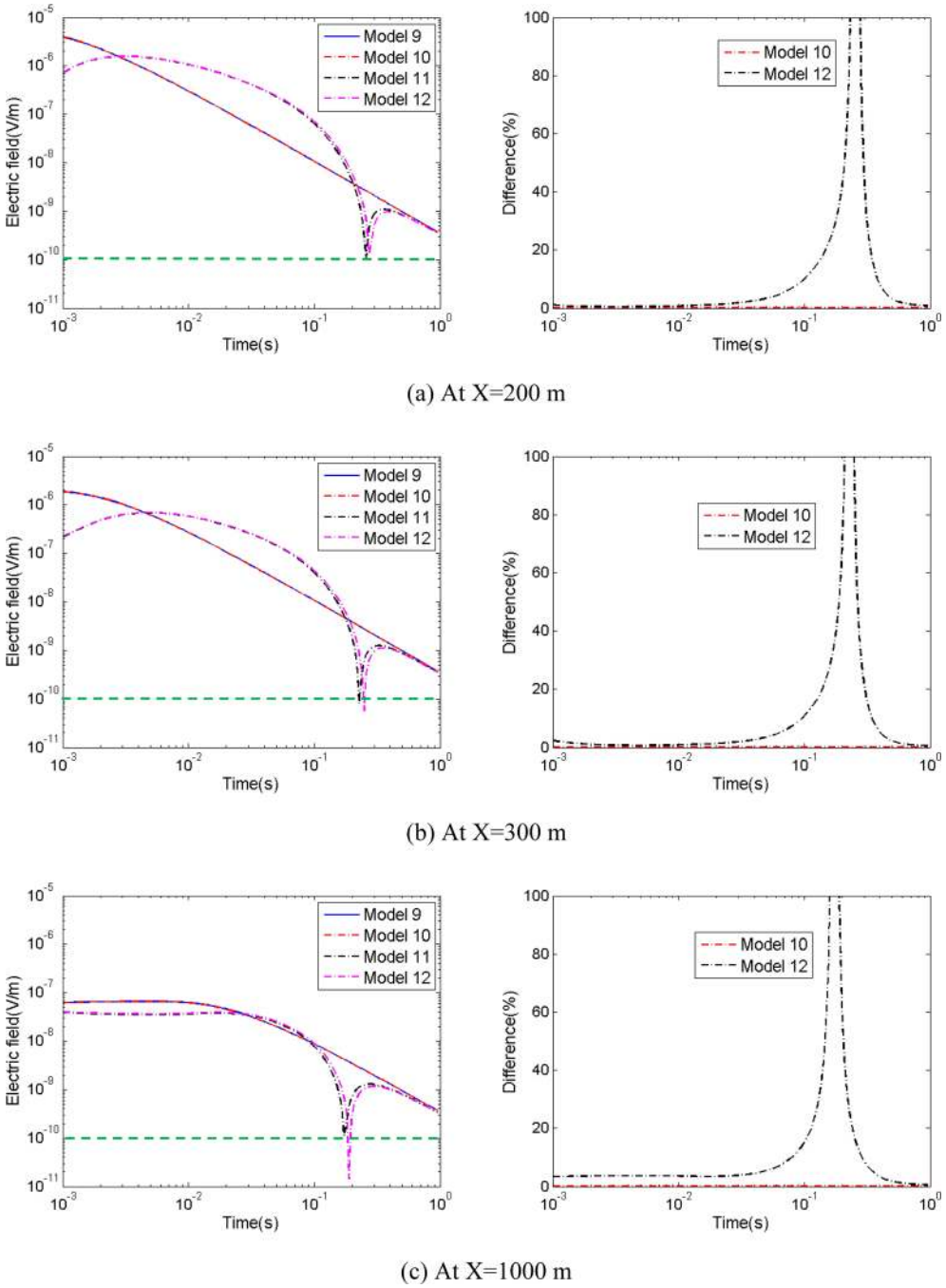

Figure 10. Inline E_x responses to the fracture models (Fig. 8 and Table 2) with and without the casing at (a) 200 m offset, (b) 300 m offset and (c) 1000 m offset. Model 9 is a background half-space model. Model 10 has the fractured zone. Models 9 and 10 correspond to Models 11 and 12, respectively, except that Models 11 and 12 have the vertical casing at their centre. A single source (Source 1) is used. The broken green lines indicate an assumed noise level.

CONCLUSIONS

We have presented a 3-D FETD modelling algorithm designed to efficiently solve a large-scale problem resulting from casing-embedded earth models. The FETD algorithm utilizes a Cholesky direct solver and a CG solver together and prevents its temporal memory usage from being doubled during the adaptive time-step process. Although unstructured tetrahedral meshes are expected to be well suited to discretizing a long round casing of a thin wall, its discretization turns out to be very expensive due to a large number of tiny elements and long mesh generation time. In order to alleviate the computational burdens, we show that a hollow steel casing can be approximated with a rectangular prism without affecting the accuracy of surface TEM responses. By avoiding discretizing the thin wall of and the curvature of the casing, the prism approximation reduces the total number of unknowns by an order of magnitude. The approximation also significantly reduces mesh generation time and improves overall mesh qualities. Owing to the efficient FETD algorithm and the prism approximation of the hollow casing, we have been able to simulate TEM responses over the 2-km long casing-embedded earth models in a reasonable timeframe. The demonstrated reductions in the computational costs may be beneficial in future inverse modelling approaches in order to aid the delineation

Downloaded from https://academic.oup.com/gji/article/202/2/901/591436 by guest on 20 August 2022

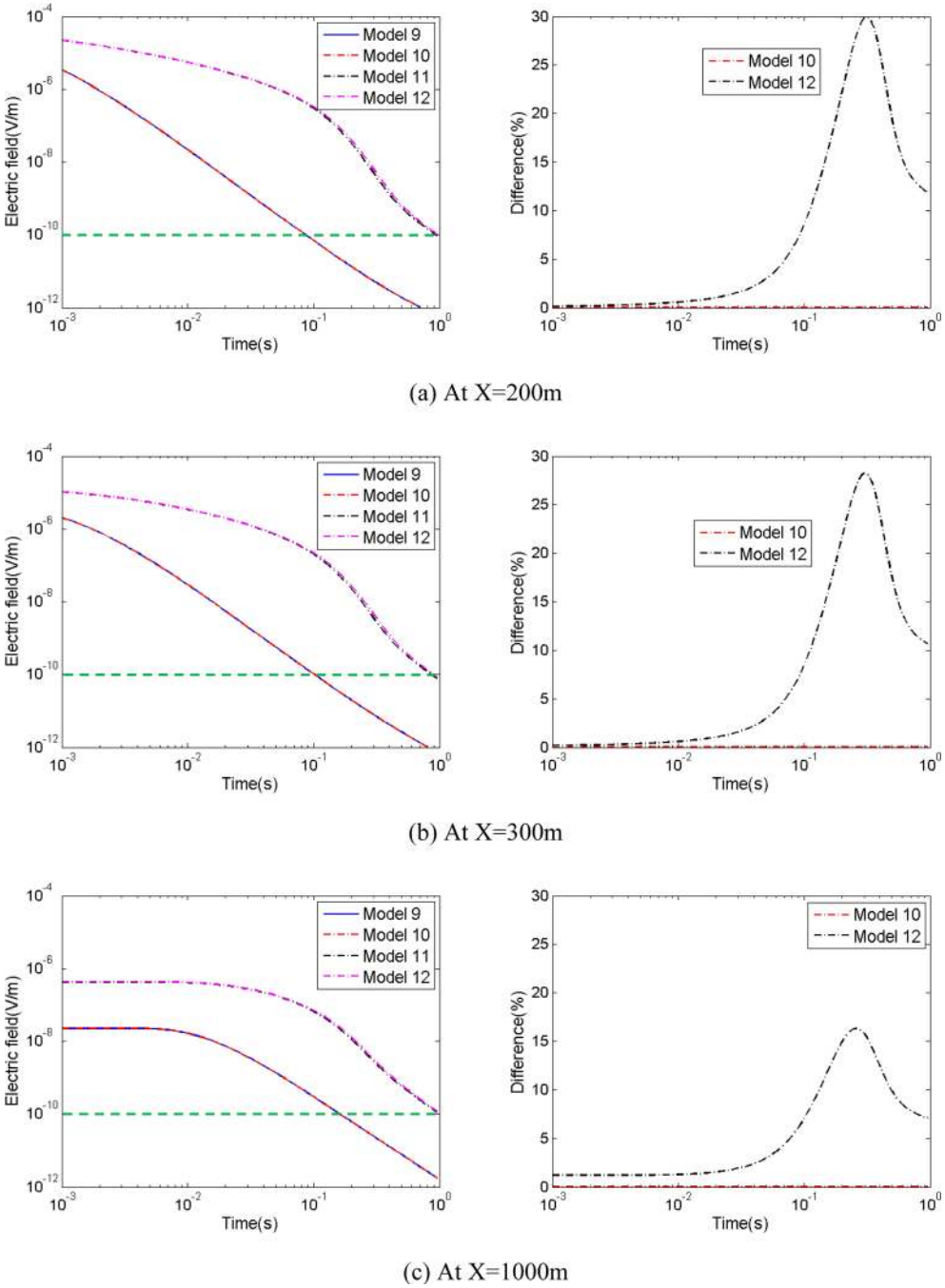

Figure 11. Inline E_x responses to the fracture models (Fig. 8 and Table 2) with and without the casing at (a) 200 m offset, (b) 300 m offset and (c) 1000 m offset. Sources 1, 2, 3 and 4 are used simultaneously. The broken green lines indicate an assumed noise level.

of the spatial distribution of fluids and fractures around the casing. When a surface source is excited around the casing, a high concentration of the transient currents diffuses through the casing and interacts with deep localized resistive/conductive targets below the casing, producing a measurable perturbation in the surface TEM fields. The anomalous fields can be measured at relatively short offsets. The concentric source array further improves the overall sensitivity of the surface TEM measurements to the targets.

In this paper, we have presented the numerical modelling works as a proof of concept. In order to use the proposed casing-aided surface-source TEM measurements in practice, we believe that it is necessary to examine spatial variations of steel-casing properties and include them into FETD modelling. Although we have assumed that the steel casing has a uniform electrical conductivity and magnetic permeability in our modelling works, a typical well consists of a number of individual steel casings with possibly different EM properties. Thus, it is advisable to address the potential effects of spatial variations of steel-casing properties on the surface TEM measurements.

Besides the proposed surface TEM configuration, we can also imagine that other EM systems such as surface-to-borehole, borehole-to-surface and crosswell configurations also have potential to take advantage of a steel-cased well as an imaginary vertical source. Pros and cons of their time-domain and frequency-domain

Downloaded from https://academic.oup.com/gji/article/202/2/901/591436 by guest on 20 August 2022

applications also need to be addressed. In short, numerical modelling of various EM configurations is desirable for further understanding the steel-casing effects and for effectively utilizing its effects for better sensing a deep localized target.

ACKNOWLEDGEMENTS

This work was carried out at Lawrence Berkeley National Laboratory and was funded by Chevron Energy Technology Company. We thank the editor Dr Ute Weckmann (Helmholtz-Zentrum), the reviewer Dr Stefan Helwig (PetroMarker) and an anonymous reviewer for constructive comments that helped us to improve the paper.

REFERENCES

Amestoy, P.R., Duff, I.S., Koster, J. & L'Excellent, J.-Y., 2001. A fully asynchronous multifrontal solver using distributed dynamic scheduling, *SIAM J. Matrix Anal. Appl.,* **23,** 15–41.

Amestoy, P.R., Guermouche, A., L'Excellent, J.-Y. & Pralet, S., 2006. Hybrid scheduling for the parallel solution of linear systems, *Parallel Comput.,* **32,** 136–156.

Balay, S. *et al.*, 2014. *PETSC Manual,* Argonne National Laboratory.

Berryman, J.G. & Hoversten, G.M., 2013. Modeling electrical conductivity for earth media with macroscopic fluid-filled fractures, *Geophys. Prospect.,* **61,** 471–493.

Caudillo-Mata, L.A., Haber, E., Heagy, L.J. & Oldenburg, D.W., 2014. Numerical upscaling of electrical conductivity: A problem specific approach to generate coarse-scale models, in *SEG Annual Meeting Abstract,* Denver, CO, pp. 680–684.

Colombo, D. & McNeice, G.W., 2013. Quantifying surface-to-reservoir electromagnetics for waterflood monitoring in a Saudi Arabian carbonate reservoir, *Geophysics,* **78,** E281–E297.

Commer, M. & Newman, G.A., 2004. A parallel finite-difference approach for three-dimensional transient electromagnetic modeling with galvanic sources, *Geophysics,* **69,** 1192–1202.

Commer, M. & Newman, G.A., 2008. New advances in three-dimensional controlled-source electromagnetic inversion, *Geophys. J. Int.,* **172,** 513–535.

Commer, M., Hoversten, G.M. & Um, E.S., 2015. Transient-electromagnetic FDTD earth modeling over steel infrastructure, *Geophysics,* **80,** E147–E162.

COMSOL, 2008. *COMSOL Multiphysics 3.5 user's guide,* COMSOL.

Fu, H., Wang, Y., Um, E., Fang, J., Wei, T. & Yang, G., 2015. A parallel finite-element time-domain method for transient electromagnetic simulation, *Geophysics,* **80**(4), E213–E224.

Gockenbach, M., 2002. *Partial Differential Equations: Analytical and Numerical Methods,* SIAM.

Goldman, M., Mogilatov, V., Haroon, A., Levi, E. & Tezkan, B., 2015. Signal detectability of marine electromagnetic methods in the exploration of resistive targets, *Geophys. Prospect.,* **63**(1), 192–210.

Heagy, L.J., Oldenburg, D.W. & Chen, J., 2014. Where does the proppant go? Examining the application of electromagnetic methods for hydraulic fracture characterization, geoconvention.com, available at: http://www.geoconvention.com/uploads/abstracts/334_GC2014_Where_does_the_proppant_go.pdf.

Helwig, S.L., Mogilatov, V.S. & Balashov, B.P., 2010. The use of a circular electric dipole source in hydrocarbon exploration, *SEG Denver Annual Meeting,* doi: 10.1190/1.3513893.

Hoversten, G.M., Commer, M., Haber, E. & Schwarzbach, C., 2014. Hydrofrac monitoring using ground time-domain EM, *76th EAGE Conference and Exhibition,* Amsterdam, WS09-C08.

Hördt, A. & Müller, M., 2000. Understanding LOTEM data from mountainous terrain. *Geophysics,* **65,** 1113–1123.

Kaufman, A.A., 1990. The electrical field in the a borehole with a casing, *Geophysics,* **55,** 29–38.

Kim, H.J. & Lee, K.H., 2006. Electromagnetic fields in a non-uniform steel-cased borehole, *Geophys. Prospect.,* **54,** 433–439.

Kim, J., Um, E. & Moridis, G., 2014. Fracture Propagation, Fluid Flow, and Geomechanics of Water-Based Hydraulic Fracturing in Shale Gas Systems and Electromagnetic Geophysical Monitoring of Fluid Migration, *SPE (Society of Petroleum Engineers) Hydraulic Fracturing Technology Conference,* 4–6 February, The Woodlands, TX, USA.

Lee, K.H., Kim, H.J. & Uchida, T., 2005. Electromagnetic fields in a steel-cased borehole, *Geophys. Prospect.,* **53,** 13–21.

Mogilatov, V. & Balashov, B., 1996. A new method of geoelectrical prospecting by vertical electric current soundings, *J. Appl. Geophys.,* **36,** 31–41.

Nédélec, J.-C., 1986. A new family of mixed elements in R3, *Numer. Math.,* **50,** 57–81.

Newman, G. & Alumbaugh, D., 1995. Frequency-domain modeling of airborne electromagnetic responses using staggered finite differences, *Geophys. Prospect.,* **43,** 1021–1042.

Pardo, D. & Torres-Verdin, C., 2013. Sensitivity analysis for the appraisal of hydrofractures in horizontal wells with borehole resistivity measurements, *Geophysics,* **78,** D209–D222.

Pardo, D., Demkowicz, L., Torres-Verdín, C. & Paszynski, M., 2007. A goal oriented hp-adaptive finite element strategy with electromagnetic applications. Part II: Electrodynamics, *Comput. Methods Appl. Mech. Eng.,* **196,** 3585–3597.

Saad, Y., 2003. *Iterative Methods for Sparse Linear Systems,* SIAM.

Schenkel, C.J. & Morrison, H.F., 1990. Effects of well casing on potential field measurements using downhole current sources, *Geophys. Prospect.,* **38,** 663–686.

Si, H., 2013. A quality tetrahedral mesh generator and 3D Delaunay triangulator, Version 1.5, User's manual. WIAS Technical Report No. 13.

Um, E., Harris, J. & Alumbaugh, D., 2010. Three-dimensional time-domain simulation of electromagnetic diffusion phenomena: a finite-element electric-field approach, *Geophysics,* **75,** F115–F126.

Um, E., Alumbaugh, D., Harris, J. & Chen, J., 2012. Numerical modeling analysis of short-offset electric-field measurements with a vertical electric dipole source in complex offshore environments, *Geophysics,* **77,** E329–E341.

Um, E., Commer, M. & Newman, G.A., 2013. Efficient pre-conditioned iterative solution strategies for the electromagnetic diffusion in the Earth: finite-element frequency-domain approach, *Geophys. J. Int.,* **193,** 1460–1473.

Wu, X. & Habashy, T.M., 1994. Influence of steel casings on electromagnetic signals, *Geophysics,* **59,** 378–390.

Downloaded from https://academic.oup.com/gji/article/202/2/901/591436 by guest on 20 August 2022